

1
2
3
4
5
6 **Evaluation of emissions and transport of CFCs using surface observations and**
7 **their seasonal cycles and the**
8 **GEOS CCM simulation with emissions-based forcing**
9

10
11 Qing Liang^{1,2}, Richard S. Stolarski¹, Anne R. Douglass¹, Paul A. Newman¹, J. Eric Nielsen^{3,4}
12
13

14 ¹ NASA Goddard Space Flight Center, Atmospheric Chemistry and Dynamics Branch, Code
15 613.3, Greenbelt, MD 20771, USA. (liang@code916.gsfc.nasa.gov,
16 Richard.S.Stolarski@nasa.gov, Paul.A.Newman@nasa.gov, Anne.R.Douglass@nasa.gov)

17 ² Oak Ridge Associated Universities, NASA Postdoctoral Program, Oak Ridge, Tennessee 37831,
18 USA.

19 ³ NASA Goddard Space Flight Center, Global Modeling and Assimilation Office, Code 610.1,
20 Greenbelt, MD 20771, USA. (nielsen@gmao.gsfc.nasa.gov).

21 ⁴ Science Systems and Applications Inc., Lanham, Maryland, USA.
22
23
24
25
26
27
28
29
30
31
32
33
34
35
36
37
38
39
40

41 Submitted to Journal of Geophysical Research – Atmospheres
42 November 15, 2007

43 Corresponding Author: Qing Liang, liang@code916.gsfc.nasa.gov
44

1 **Abstract**

2 Levels of ozone depleting substances (ODSs) in our atmosphere are determined by
3 production, emission, and loss processes. However, atmospheric models are forced by the
4 specified levels of these ODSs rather than the more fundamental emissions-based forcing. To
5 more accurately represent the physics and chemistry of climate change on atmospheric
6 circulation and ODS, and therefore future ozone recovery, it is desirable to switch from the
7 current highly constrained mixing-ratio-based forcing to emissions-based forcing in general
8 circulation models (GCMs). As a first step of this model transition, we have conducted a 45-year
9 (1960-2005) emissions-based simulation of the three primary chlorofluorocarbons (CFC-11, -12,
10 -113) using the GEOS coupled chemistry-climate model (CCM). The simulated CFC
11 concentrations and their seasonal cycles are compared with the observations to evaluate
12 emissions and atmospheric transport. The simulated CFC-12 agrees well with the observations,
13 indicating a good estimate of emission and atmospheric loss. The simulated CFC-11 shows a
14 high bias, particularly after 1990 due to an overestimate of emission from banks. Emission of
15 CFC-113 is 15% too high, resulting in a consistent 18% high bias in surface concentrations.
16 Surface observations of CFCs at many AGAGE and NOAA-GMD sites show significant
17 seasonal variations. Using tagged CFC tracers to track recent surface emissions and aged air
18 masses transported downward from the stratosphere separately, we quantify the relative
19 contribution of stratosphere-troposphere exchange (STE) and tropospheric transport to the
20 seasonal cycles of CFCs in the lower troposphere. The lower troposphere seasonal cycles of
21 CFCs are dominated by tropospheric transport of recent emissions during 1985-1994 with peak-
22 to-trough amplitude of as much as 6 pptv for CFC-11, 10 pptv for CFC-12, and 3 pptv for CFC-
23 113. The 1995-1999 period marks the transition period when variations due to fresh emissions

1 and STE become equally important. Seasonal cycles of CFCs at most surface sites in the 2000-
2 2004 period are dominated by STE. Seasonal cycles of CFCs due to STE show a late
3 winter/early spring maximum and a summer/fall minimum, with amplitudes of ~4-5% of
4 absolute mixing ratios at the surface. Seasonality of the tropospheric transport component at
5 individual stations is governed by seasonal transport variations of fresh emissions from the
6 polluted regions.

1
2
3
4
5
6
7
8
9
10
11
12
13
14
15
16
17
18
19
20
21
22
23
24
25

1. Introduction

While current coupled chemistry climate models (CCM) are forced by specifying surface mixing ratios recommended by the World Meteorological Organization (WMO)/United Nations Environmental Program (UNEP), recent modeling studies show that increasing greenhouse gases will speed up the mean atmospheric circulation and result in shorter mean age of air [e.g. *Austin and Li, 2006; Butchart et al., 2006; Douglass et al., 2007*]. This suggests that ozone-depleting substances (ODS) will be removed more quickly in a future climate [*Butchart and Scaife, 2001*]. Therefore, to accurately predict the future ozone (O₃) recovery and its interaction with climate change, it is desirable to advance from the current commonly-adopted mixing-ratio-based forcing to emissions-based forcing in CCMs. One major difficulty in implementing this model transition is demonstrating the model's adequacy in simulating the mean atmospheric circulation and the atmospheric lifetimes of ODS. A model with a poor circulation will not simulate well the annual atmospheric loss, leading to an inaccurate projection of the future ODS concentrations and stratospheric ozone. An additional difficulty lies in the uncertainties of the emissions of ODS, e.g. chlorofluorocarbons (CFCs) and hydrochlorofluorocarbons (HCFCs). Even with well-regulated man-made ODS like CCl₃F (CFC-11, trichlorofluoromethane) and CCl₂F₂ (CFC-12, dichlorodifluoromethane), there are significant differences in emission estimates from the existing unvented air conditioners, refrigerators, and plastic foams (referred to as "banks") [*Chapter 1, WMO 2003; Daniel et al., 2007*]. Emission estimates made using a "bottom-up" approach, e.g. estimates from *Intergovernmental Panel on Climate Change (IPCC) [2005]*, are based on production and release rates, therefore subject to uncertainties in the bank sizes, annual release rates and service lifetimes of banks [*McCulloch et al., 2001*]. Another type of estimate derives a CFC emission with box models that use the reported production, observed atmospheric

1 CFC concentration and that CFC's lifetime as constraints (top-down approach), e.g. *WMO*
2 [2003]. With such an approach, uncertainties arise due to systematic reporting errors as well as
3 uncertainty in the atmospheric lifetimes of the various CFC [*Daniel et al.*, 2007].

4 As a first step of transition from a mixing-ratio-based CCM to an emissions-based CCM, we
5 have conducted an emissions-based simulation of the three principal CFCs (CFC-11, CFC-12,
6 and $\text{CCl}_2\text{FCCIF}_2$ (CFC-113)). CFC simulations provide a good initial effort for tackling the
7 emissions problem for two reasons: i) simple chemistry: CFCs are destroyed in the middle and
8 upper atmosphere through photolysis with well-known rates, ii) single source: CFCs are man-
9 made pollutants released at the surface with reasonably good-reported production and emission
10 release rates, in contrast to many other ODSs that have natural sources and emissions that are
11 highly uncertain.

12 Surface CFC observations at many Advanced Global Atmospheric Gases Experiment
13 (AGAGE) sites show prominent seasonal cycles [*Prather et al.*, 1987; *Prinn et al.*, 2000]. Early
14 studies have attributed seasonal variability to tropospheric transport and interhemispheric
15 exchange [*Prather et al.*, 1987; *Prinn et al.*, 2000]. *Nevison et al.* [2004] suggested that due to
16 the phase-out of CFCs in the 1990s, observed CFC seasonality in the tropospheric surface
17 stations after mid-1990s should primarily reflect stratosphere troposphere exchange (STE) via
18 the stratospheric Brewer-Dobson circulation. Using the Whole Atmosphere Community Climate
19 Model (WACCM) with mixing-ratio-based forcing, they investigated the seasonality of CFCs in
20 the troposphere and concluded that stratosphere exerts a coherent influence on the tropospheric
21 CFC mixing ratios. A model's ability to reproduce the amplitude and phase of the seasonal cycle
22 of CFCs in the troposphere is a useful indicator of its capability to simulate the atmospheric
23 transport. In addition, many other long-lived atmospheric trace gases, i.e. N_2O and CO_2 that are

1 important in the projection of ozone recovery and climate change, show similar seasonality as
2 CFCs due to the same governing atmospheric transport processes [*Shia et al.*, 2006; *Jiang et al.*,
3 2007]. A good understanding of the seasonality of CFCs is useful in source characterization of
4 these trace gases.

5 Here we present results from a 45-year (1960-2005) emissions-based simulation of CFC-11,
6 CFC-12, and CFC-113 using the 3-dimensional GEOS Chemistry Climate Model (GEOS CCM)
7 [*Stolarski et al.*, 2006; *Pawson et al.*, 2007 (JGR submitted)]. We use the simulated CFCs to
8 evaluate the model's atmospheric circulation plus the magnitude and distribution of CFC
9 emissions. The model description and a summary of observations used are included in section 2.
10 The simulated CFCs are compared with observations in section 3. Discussion of seasonal cycles
11 of CFCs in the troposphere and its implications on simulated atmospheric transport and CFC
12 emission distributions is presented in section 4, followed by summary and discussions in section
13 5.

14 **2. Model and observations**

15 **2.1 Model description**

16
17
18 We have conducted a 45-year emissions-based simulation of CFC-11, CFC-12, and CFC-113
19 from January 1960 to December 2004 using the Goddard Space Flight Center (GSFC) GEOS
20 CCM, described by *Stolarski et al.* [2006] and *Pawson et al.* [2007]. The 1 January 1960 initial
21 condition of CFC mixing ratios and other atmospheric constituents is taken from a prior mixing-
22 ratio-based simulation. The horizontal resolution of the simulation is 2° latitude by 2.5°
23 longitude, with 55 layers extending from the surface to 0.01 hPa. The GEOS CCM couples the
24 GEOS-4 GCM [*Bloom et al.*, 2005] with a stratospheric chemistry module [*Douglass et al.*,
25 1996]. A comprehensive evaluation of several CCM simulations of the period 1960-2005 shows

1 that the GEOS CCM simulation agrees well the observations in many of the meteorological,
2 transport-related, and chemical diagnostics [Eyring *et al.*, 2006]. Pawson *et al.* [2007] further
3 validate the GEOS CCM ozone and temperature with the observations and show the strengths of
4 the model in simulating ozone, temperature, and the temperature-ozone coupling. Douglass *et al.*
5 [2007] show that GEOS CCM reproduces well the atmospheric circulation with realistic age-of-
6 air, and therefore a realistic loss and atmospheric lifetime for CFC. Waugh *et al.* [2007] also
7 show good simulations of mean age and CFC profiles in comparison to observations.

8 The GEOS CCM simulation couples the mixing-ratio-based ODS, including CFCs, into the
9 radiation code. The Cl_y in the chemistry simulation comes from the mixing-ratio-based CFCs.
10 The simulation also includes three independent tracers: CFC-11, 12 and 113 calculated with
11 specified emissions. These are transported by the CCM circulation and removed by photolysis
12 and reaction with $O(^1D)$ in the middle and upper atmosphere with the same rates as the mixing-
13 ratio-based CFCs, but they do not feedback into the radiative heating code. In addition, while
14 the emissions-based CFCs may differ from the mixing-ratio-based CFCs, the difference does not
15 feedback on Cl_y or ozone.

16 Emissions of CFCs are released at the lowest layer in the model based on the bottom-up
17 emission estimates of CFCs from McCulloch *et al.* [2001, 2003]. Historically, CFC-11 was used
18 primarily in aerosol propellant mixtures with prompt release to the atmosphere within a year
19 after production but later mainly used in rigid plastic insulating foams of which leakage is small
20 and slow [McCulloch *et al.*, 2001]. CFC-12 was used primarily within refrigeration and air
21 conditioning systems with additional usage as aerosol propellants [McCulloch *et al.*, 2003].
22 CFC-113 was used as a solvent and cleaning agent for electronics and metal [Environmental
23 Protection Agency (EPA), 1980]. The annual global emissions of CFC-11, CFC-12, and CFC-

1 113 for each year between 1960 and 2005 are shown in Figure 1. In our simulation, we release
2 CFCs with the same magnitude throughout the year, assuming no seasonal dependence. We
3 deploy a regional distribution of CFC-11 and CFC-12 according to the fractions of world total
4 production for individual countries as described in *McCulloch et al.* [2001, 2003], *the Alternative*
5 *Fluorocarbons Environmental Acceptability Study* (AFEAS) (<http://www.afeas.org>, 2001), and
6 WMO [2003]. 89% of the CFC-12 and 98% of the CFC-11 are emitted in the Northern
7 Hemisphere (NH), with the remaining released in the Southern Hemisphere (SH). An example
8 distribution of CFC-11 for 2000 is shown in Figure 2. There is no other ready-to-use regional
9 distribution of CFCs, therefore we adopt the same distribution fraction for 2000 throughout the
10 entire simulation period. For CFCs that have long atmospheric lifetimes (>45 years), compared
11 to an interhemispheric exchange time of a few months in the tropics [e.g. *Bowman and Cohen*,
12 1997; *Gupta et al.*, 2001] to ~1 year for mixing to the extratropics [*Bowman and Cohen*, 1997],
13 we do not expect this to affect the long-term simulation of atmospheric CFCs. However, the
14 resulting simulation biases need to be kept in mind when comparing the simulated results with
15 the interhemispheric gradient and with observed CFCs at the individual surface stations.

16 To quantitatively understand the relative contribution of stratosphere-troposphere exchange
17 (STE) and tropospheric transport to the seasonal cycle of CFCs in the troposphere, we have also
18 added two sets of tagged tracers in the simulation, one set of tropospheric tracers to track CFCs
19 that have been recently emitted (CFC-11T, CFC-12T, CFC-113T) and another for CFCs that
20 were at some time in the stratosphere (CFC-11S, CFC-12S, CFC-113S). The two sets are
21 transported as independent tracers in the CCM. Fresh CFCs emitted at the surface are labeled as
22 “tropospheric CFC tagged tracers” and being transported in the CCM circulation. When the
23 tropospheric tagged tracers are transported across the tropopause into the stratosphere, they

1 become “stratospheric CFC tagged tracers”. The majority of these stratospheric tracers
2 circulates through the middle and upper atmosphere and re-enters the troposphere via STE.
3 However, these tracers keep their identities as stratospheric tracers to separate the old CFCs from
4 new emissions. Since the regional emission distribution is for 2000, we limit our tagged
5 simulation between January 1995 and December 2004 for a meaningful comparison between the
6 simulations and the observations. Initial concentrations of tropospheric and stratospheric tracers
7 for the tagged simulation are obtained with a 5-year spin-up before 1995 to obtain a reasonable
8 partition between the two.

9 10 **2.2 Observations**

11 Long-term observations of CFC-11, CFC-12, and CFC-113 are made by the Advanced
12 Global Atmospheric Gases Experiment (AGAGE) and the National Oceanic and Atmospheric
13 Administration – Global Monitoring Division (NOAA-GMD). The AGAGE measurements were
14 obtained using the Hewlett-Packard gas chromatograph (GC) Instrument with precisions of 0.1-
15 0.3% [Prinn *et al.*, 2000]. The AGAGE data are divided into three subsets, the Atmospheric
16 Lifetime Experiment (ALE), the Global Atmospheric Gases Experiment (GAGE), and the
17 AGAGE [Prinn *et al.*, 2000], and includes five locations: 1) Ireland, Adrigole (ADR, 1979-1983)
18 and Mace Head (MCH, 1987-present); 2) U.S. West Coast, Cape Meares, Oregon (CME, 1979-
19 1989) and Trinidad Head, California (TRH, 1995-present); (3) Ragged Point, Barbados (RGP,
20 1978-present); (4) Cape Matatula, American Samoa (MAT, 1978-present); (5) Cape Grim,
21 Tasmania (CGR, 1978-present) (Figure 2, Table 1).

22 The NOAA-GMD observations are obtained at 10 sites: (1) Alert (ALT), (2) Barrow (BRW),
23 (3) Park Falls (LEF), (4) Harvard Forest (HFM), (5) Niwot Ridge (NWR), (6) Grifton (ITN), (7)
24 Cape Kumukahi (KUM), (8) Mauna Loa (MLO), (9) Tutuila (SMO), (10) South Pole (SPO).

1 The NOAA-GMD observations include flask data from 1977 to current, Chromatograph for
2 Atmosphere Trace Species (CATS) data from 1988 to 1999, and Radiatively Important Trace
3 Species (RITS) data from 1999 to current [*Montzka et al.*, 1999; *Thompson et al.*, 2004]. The
4 locations of the stations are shown in Figure 2. Detailed geographical and instrument
5 information at each sites are listed in Table 1.

6

7 **3. Simulated results and evaluation of the emission estimates**

8

9 Figure 3 shows the observed and simulated surface monthly mean CFCs in the NH and SH
10 between January 1960 and December 2004. The simulated CFC-12 (top) agrees well with the
11 observation in both hemispheres and the average differences (simulation-observation) are -0.1%
12 in the NH and -0.6% in the SH, with annual biases (simulation-observation) range from -2.4% to
13 1.6%, comparable to the 2% differences between the independent laboratory measurements
14 [*WMO*, 2007]. This indicates that the simulation presents a good estimate of annual emissions
15 and photolytic loss in the stratosphere.

16 The simulated CFC-11 (middle) in the NH shows a high bias and the overestimate increases
17 from an average of 4.9 pptv (+2.7%) in 1978–1984 to 10.4 pptv (+4.1%) in 1985-1994 and 18.1
18 pptv (+6.9%) in 1995-2004. The simulated CFC-11 in the SH agrees well with the observation
19 before 1989, with annual differences < 3.5 pptv (+1.5%), but the overestimate increases
20 significantly afterwards and reaches an average of 15.6 pptv (+6.0%) in 1995-2004.

21 The simulated CFC-113 (bottom) in both hemispheres is consistently higher than
22 observations with the overestimate steadily increasing from 4.5 pptv (+11.3%) in the NH and 3.8
23 pptv (+12.9%) in the SH in 1984 to peak values of 18.0 pptv (+22.2%) in the NH in 1992 and
24 15.8 pptv (+19.2%) in the SH in 1995. As the emissions decrease rapidly after the early 1990's

1 (Figure 1), the simulation overestimate also decreases (+17.0% and +16.7% in NH and SH,
2 respectively, for 1995-2004).

3 Comparison between the simulated and observed CFCs at individual surface sites is
4 consistent with the comparison between the hemispheric means. Figure 4 shows the mid-latitude
5 sites, Adrigole/Mace Head in the NH and Cape Grim in the SH. The model reproduces well the
6 observed CFC-12 at both sites (top panels), with negligible low biases, -3.4 pptv (-1.0%) at
7 Adrigole/Mace Head and -5.5 pptv (-1.2%) at Cape Grim, respectively. The simulated CFC-11
8 biases (middle panels) increases slowly from an average of +4.2 pptv (+2.3%) at Adrigole/Mace
9 Head and +1.0 pptv (+0.6%) at Cape Grim before 1985 to +21.3 pptv (+8.2%) and +7.6 pptv
10 (6.8%) in 1995-2004, respectively. The model CFC-113 (bottom panels) is consistently higher
11 than the observations, with average biases of +15.4 pptv (+19.3%) at Mace Head and +11.4 pptv
12 (+16.7%) at Cape Grim between 1983 and 2004.

13 We diagnose the simulation biases in CFC concentrations by examining the simulated CFC
14 atmospheric lifetimes. We calculate the photolysis rates offline using the archived overhead
15 nitrogen (N_2), oxygen (O_2), and O_3 column, and the reaction rates of $CFC + O(^1D)$ using the
16 saved $O(^1D)$ concentration and temperature fields. The average lifetimes of CFC-11 and CFC-12
17 calculated in the GEOS CCM are 57 years and 100 years, respectively, with photolysis
18 accounting for > 99% of the loss. CFC-113 has a lifetime of 97 years, with 90% of the loss due
19 to photolysis and 10% via reaction with $O(^1D)$.

20 The accurate simulation of the observed CFC-12 mixing ratios and an atmospheric lifetime
21 of 100 years, similar to that in Chapter 1, Table 1-4., in the *WMO* [2007] assessment, suggests
22 reasonable arctic fluxes, and hence photolytic loss of CFCs, in model [*Dougllass et al.*, 2007;
23 *Waugh et al.*, 2007]. These accurate simulations are essential to correctly simulating the

1 atmospheric transport, fractional release, and photochemical age of CFCs [Douglass *et al.*, 2007].
2 The aforementioned implies that the overestimate in CFC-11 mixing ratios is probably due to an
3 overestimate of emissions from banks. Compared with CFC-12 (most of its bank resides as
4 refrigerants with an average characteristic release time of 3-5 years), more than 90% of the CFC-
5 11 banks are in close-cell plastic foams with complex and highly variable immediate release
6 fractions from 4% to 95%, leaking rates from 0.5% to 5% yr⁻¹, and service time from 12 to 50 yr
7 [McCulloch *et al.*, 2001]. All these uncertainties propagate into the emission estimates. The
8 result is large uncertainty in the CFC-11 emission rate, especially when the primary usage
9 switches from aerosol propellants to plastic foam blowing agents. This is consistent with our
10 simulation results that show increasing overestimate in CFC-11 after 1990, when emissions of
11 CFC-11 are dominated by release from plastic foam banks.

12 Unlike CFC-11 with significant quantities stored in the banks, 99% of CFC-113 is released to
13 the atmosphere within 6 months of sale and has negligible banks [AFEAS, 1995; Fisher and
14 Midgley, 1993]. CFC-113 emission is estimated using the fraction of CFC-113 in total CFCs in
15 the AFEAS database and scaled up accordingly based on the total CFCs in the UNEP database to
16 include additional emissions from “non-reported” countries, e.g. China, Czech Republic, India,
17 Korea, Taiwan, Romania, and Russia [McCulloch *et al.*, 2001]. This derivation method could
18 introduce error in emission estimates if the fractional composition of individual CFCs is different
19 between the reported AFEAS database and the non-reported countries. The two possible
20 contributors for the high concentrations of CFC-113 in the simulation are overestimates of
21 emissions and/or underestimates of losses. We compare the model-simulated CFC-113 burden
22 in the atmosphere with observations in Figure 5. As >90% of the burden resides in the
23 troposphere and CFC-113 concentration is relatively uniform in the troposphere, the surface

1 mixing ratio of CFC-113 is well-correlated ($r=0.9999$ in the model) with the total atmospheric
2 burden. We infer the observed burden from the observed surface observations using a model-
3 derived relationship:

$$4 \quad CFC-113 \text{ burden (Tons)} = -0.96 \times 10^4 + 3.27 \times 10^4 \times CFC-113 \text{ surface mixing ratio (pptv)}$$

5 Before 1983 when CFC-113 observations are unavailable, surface CFC-113 concentrations
6 recommended by A1B scenario of the *WMO* [2003] are used instead. The simulated CFC-113
7 burden exceeds the observed burden in 1964 and the overestimate continues to increase until
8 reaching a maximum of 23% in 1990, coincides with the emission maximum in 1989. If we
9 decrease the CFC-113 lifetime from the simulated 97 years to 50 years, the calculated
10 atmospheric CFC-113 burden matches the observed burden in 2004 while the accumulation rate
11 before 1994 and decrease rate after 1994 are too fast compared with observations. When
12 emission is decreased to 85% of what is used in the simulation, the calculated atmospheric
13 burden agrees well with observations between 1960-2004, indicating that the overestimate of
14 CFC-113 in the simulation is most likely due to overestimate in emission.

15 The CFC interhemispheric gradients are governed by the NH-SH emission partitioning, the
16 tropospheric exchange rate between hemispheres, and the relative strength of the STE from the
17 stratosphere in both hemispheres. The observed interhemispheric differences decrease from
18 1980's (21.2 pptv, 12.9 pptv, and 6.8 pptv for CFC-11, -12, and -113, respectively) to 1990's
19 (11.7 pptv, 6.4 pptv, and 3.0 pptv for CFC-11, -12, and -113, respectively) (Figure 3), consistent
20 with the change in emissions (Figure 2). The interhemispheric difference of CFC-12 in the
21 simulation agrees relatively well with the observations (an average of 23.9 pptv in 1980's and
22 14.8 pptv in 1990's) (Figure 3), indicating a good estimate of the hemispheric fractions of
23 emissions and also that the fraction has remained relatively constant (~90% in the NH and ~10%

1 in the SH) throughout the past few decades. The simulated CFC-11 hemispheric difference (18.5
2 pptv in 1980s' and 9.4 pptv in 1990s') is ~40% too high compared to observations. This
3 together with the fact that there is an overestimate in the NH before 1989 with no systematic bias
4 in the SH implies the 0.98-0.02 NH-SH emission partition fraction from year 2000 is too high for
5 the 1980s' and possibly 1990s' as well. The simulated CFC-113 hemispheric gradients in the
6 model are 9.9 pptv in 1980s' and 4.6 pptv in 1990s', 50% higher than the observations (Figure 3).
7 This overestimate could be due to both an overestimate in the NH-SH emission partition fraction
8 and overestimate in emission. Both the observed and simulated gradients of CFC-113 decrease
9 to 0.3 pptv in 2000-2004 as emission becomes negligible.

10

11 **4. Seasonal cycle of CFCs**

12

13 To examine the seasonality of CFCs at ground-based stations, we remove long-term
14 variations from the observed and simulated CFCs, as well as the CFC tagged tracers, by applying
15 a 13-month high-pass filter which uses a 13-month boxcar average algorithm. The filtered
16 monthly mean anomalies are averaged for each month of the year to obtain the long-term
17 climatological seasonal cycles. Figure 6 shows the CFC-12 time series (top) and filtered
18 anomalies (bottom) between 1995 and 2004 for two example sites, Mace Head (Figure 6a) in the
19 NH and Cape Grim in the SH (Figure 6b). The simulation reproduces relatively well the
20 observed seasonal variations of CFC-12 at the NH Mace Head site (Figure 6a) between 2000-
21 2004, but shows a phase-delay of a few months during 1995-1999. The bias in simulating the
22 phase of seasonality during 1995-1999 is also present at a few other NH mid-latitude sites,
23 Trinidad Head, Mauna Loa, and Cape Kumukahi (not shown), which are heavily influenced by
24 continental pollution outflow. The simulated seasonal cycle of CFC-12 at the SH Cape Grim, as

1 well as two other SH sites (not shown), agrees with the observations both in magnitude and
2 phase. Due to rapid decreases in emissions in North America and Europe in the 1990s, the
3 regional emission distribution has changed significantly from 1990s to 2000s. Error in regional
4 emission distribution is likely to introduce bias in simulating the seasonal variation of
5 tropospheric transport of fresh CFCs to the above NH sites. Model transport errors may also
6 contribute to the biases. Therefore, we first limit our comparison of simulated vs. observed
7 seasonal cycles for 2000-2004 and then examine how seasonal cycles of CFCs change as
8 emissions change from 1985 to 2004 to understand the governing processes of CFC seasonality
9 and the possible causes of simulation biases.

10 **4.1 Seasonality of surface CFCs and governing processes**

11 The 5-year averaged seasonal cycles of CFCs and the tagged tracers for 2000-2004 are
12 shown at four selected stations in the NH in Figure 7a and three stations in the SH in Figure 7b.
13 Significant seasonal variability of CFCs is observed at many surface stations. Observed CFCs
14 show a late winter/early spring maximum (January-February in NH and September-October in
15 SH) and a summer/fall minimum (July-September in NH and March-May in SH) (Figure 7a and
16 7b). The amplitudes (maximum-minimum) of the seasonal cycles of the CFCs are ~4% (~2 pptv
17 for CFC-12, ~1 pptv for CFC-11, and ~0.4 pptv for CFC-113) of the absolute mixing ratios at the
18 NH sites and reduce to ~2% at the SH sites. The simulation reproduces well the observed phase
19 and amplitude of the seasonal cycles of CFC-11 and CFC-12 at most of the observation sites.
20 The seasonal maxima/minima of simulated CFC-113 at most stations is shifted 1-2 months from
21 that observed, and amplitudes of the seasonal variations are underestimated.

22 We further decompose the seasonal cycle of CFCs to quantify the contributions of
23 stratosphere-to-troposphere transport of old air and tropospheric transport of recent emissions

1 between 2000-2004 by examining the two sets of tagged tracers (Figure 7a and 7b). Seasonal
2 variations of CFC-11 and CFC-12 at the surface sites are dominated by variations of the
3 stratospheric components (CFC-11S and CFC-12S) throughout the globe, except at the southern
4 tropical sites - Tutuila, American Samoa, with contributions from tropospheric transport (CFC-
5 11T and CFC-12T) varying from a comparable magnitude to almost zero at individual sites.
6 Seasonality of CFC-11 and CFC-12 at Tutuila is dominated by the tropospheric component due
7 to active NH-to-SH transport. The simulated seasonal variation of CFC-113 closely follows that
8 of CFC-113S as emissions are negligible, resulting in very small values (<0.1 pptv) of CFC-
9 113T during 2000-2004.

10 The stratospheric tracers show early spring maxima and early fall minima in both
11 hemispheres. The amplitudes of the seasonal cycles of the stratospheric CFC tracers are largest
12 in the NH mid- and high latitudes: ~2.0 pptv for CFC-12S, ~1.6 pptv for CFC-11S, and ~0.4
13 pptv for CFC-113S. The amplitudes reduce by half in the NH tropics and the SH mid- and high
14 latitudes, and are small in the SH tropics.

15 The seasonal variations in the stratospheric component of CFCs are associated with the STE
16 [Nevison *et al.*, 2004]. The winter downwelling of old, CFC-depleted air from the middle and
17 upper stratospheric results in a CFC seasonal minimum in the polar lower stratosphere (the blue
18 anomalies in Figure 8). The amplitude of the associated seasonal variations is stronger in the
19 northern hemisphere compared with the southern hemisphere because of the stronger mixing
20 rates and downward Brewer-Dobson stratospheric circulation [Holton *et al.*, 1995; Nevison *et al.*,
21 2004]. In the NH, the seasonal cycle in the lower stratosphere slowly migrates to the troposphere.
22 The descent in the Arctic has a seasonal minimum anomaly of -6 pptv in April-May in the near
23 tropopause region (Figure 9b). However, it is difficult for stratospheric air masses to penetrate

1 into the Arctic lower troposphere [*Stohl et al.*, 2006; *Law et al.*, 2007]. The lower tropospheric
2 minimum occurs in July-August (Figure 9a), approximately 3 months behind the near tropopause
3 region's minimum and 4-5 months behind the lower stratosphere one. The amplitude of the
4 seasonal cycle near the surface is significantly reduced (1 pptv for CFC-12) compared to the
5 lower stratosphere (70 pptv) and near tropopause region (5-10 pptv). This seasonal minimum
6 near the surface is reached in the NH extra-tropics in the mid-summer (July-August period in
7 Figure 9a). The surface minimum in the SH is weaker than the NH, the downward migration
8 from the lower stratosphere to the upper troposphere is also weaker and slower in the SH (Figure
9 8cd and 9). The surface minimum in both hemispheres is consistent with net mass flux out of the
10 stratosphere during the Spring and early Summer [*Olsen et al.*, 2004]. Furthermore, the weaker
11 annual cycle in the SH is also consistent with the weaker SH mass flux out of the stratosphere
12 [*Olsen et al.*, 2004].

13 Since emissions have decreased rapidly after the early 1990s' and reduced to very low levels
14 by 2000, the percentage contribution of recent emissions (<4%) to the tropospheric burden of
15 CFC-12 is minor compared to aged emission that has circulated through the stratosphere (Figure
16 6). However, tropospheric transport of recent emissions still contributes significantly to the
17 seasonal cycles in the lower troposphere (Figure 7). Figure 10 shows the annual-mean global
18 distribution of the simulated tropospheric tracer, CFC-12T, averaged between 0-2 km for 2000.
19 In the NH, distribution of CFC-12T in general follows the emissions with hot spots of high
20 mixing ratios concentrated in the high emission regions, i.e., Europe, China, and the eastern
21 United States (Figure 2). CFC-12T in the NH mid- and high latitudes shows a seasonal variation
22 of ~ 1 pptv, 5-10% of the absolute mixing ratios, with a maximum in winter as surface emissions
23 are capped in the lower troposphere by strong subsidence during winter, in particularly over

1 Europe and Asia [Stohl *et al.*, 2002; Liang *et al.*, 2004; Stohl, 2006]. In addition, mixing ratios
2 of the tropospheric component of CFCs at individual stations vary as winds vary in strength and
3 direction in individual seasons, bringing air from different continents that differ in CFC levels as
4 the emission magnitudes are different. In the tropics, 10°N-20°S, CFC-12T mixing ratios exhibit
5 significant seasonality (~1 pptv) with maximum during NH winter due to the NH-to-SH
6 transport which occurs primarily in the near-surface layer in winter [Gupta *et al.*, 2001]. In the
7 SH, distribution of CFC-12T is zonally uniform. Mixing ratios decrease poleward, and exhibit
8 little seasonal variation.

9 The GEOS CCM simulates well the seasonality associated with STE [Olsen *et al.*, 2004] and
10 the NH-to-SH transport, therefore reproduces well the amplitude and phase of seasonal cycles of
11 CFC-11 and CFC-12 at sites that are dominated by these two processes, i.e. Park Falls, Tutuila,
12 Cape Grim, South Pole (Figure 7). At several NH observation sites where long-range
13 hemispheric transport contributes significantly to the seasonality of CFCs, the simulated seasonal
14 cycles of CFC-11 and CFC-12 show a slight phase-shift or overestimate in amplitude, suggesting
15 biases associated with emission distribution and tropospheric meteorological transport. The
16 biases in the simulated CFC-113 are more apparent (Figure 7). The phase and percentage
17 amplitude of CFC-113S agrees well with those of CFC-11/CFC-12, indicating well simulated
18 seasonality due to STE. A significant increase in the amplitude of CFC-113T is needed to
19 reconcile the difference between the observed and simulated CFC-113 seasonal cycles. This
20 suggests that the current emission estimate of CFC-113 for 2000-2004 is too small.

21 **4.2 Evolution of CFC seasonality and implications for emissions**

1 In this subsection, we examine how the annual cycles of CFCs have changed between 1985
2 and 2004 as emissions decreased. We focus on five surface sites in the NH and one in the SH
3 that have accumulated a relatively long and continuous record of CFC levels.

4 Figure 11 shows the 5-year averaged seasonal cycles of CFC-11 for 1985-1989, 1990-1994,
5 1995-1999, and 2000-2004 (CFC-12 is similar). Note that the magnitude of seasonality of the
6 stratospheric tracers of CFCs is proportional to their atmospheric loading as governed by the
7 Brewer-Dobson circulation. Since the concentration of CFCs in the middle and upper
8 atmosphere during 2000-2004 is comparable or larger than the earlier years, the amplitude of
9 CFC-11 seasonality due to STE should be ≤ 1.6 pptv in NH (≤ 1 pptv in SH) before 2000. During
10 1985-1994, seasonal amplitude of CFC-11 reaches ~ 4 -5 pptv at the NH stations, implying that
11 the seasonal variation of CFC-11 is dominated by fresh emissions. As emission decreases,
12 seasonal variation of CFC-11 is significantly reduced in amplitude. 1995-1999 marks the
13 transition period when both tropospheric transport and STE contribute significantly to the
14 seasonal cycles of CFC-11 at the surface. Seasonal variation of CFC-11 is dominated by STE
15 during 2000-2004 (section 4.1).

16 The hemispheric transport of anthropogenic emissions from adjacent populated continents to
17 the remote AGAGE/GMD sites contributes to the observed seasonality of carbon monoxide (CO)
18 [e.g. *Cape et al.*, 2000; *Li et al.*, 2002; *Heald et al.*, 2003; *Liang et al.*, 2004]. Since
19 anthropogenic emissions of CO and CFCs share common source regions, the contribution of
20 emissions from different regions to the seasonality of CO at the remote observation sites together
21 with the evolution of observed CFCs seasonality lends valuable information in understanding the
22 magnitude of regional emissions of CFCs over Europe, North America, and Asia.

1 Mace Head (Fig. 11, top row, middle) is mostly influenced by anthropogenic emissions from
2 Europe [*Simmonds et al.*, 1997; *Cape et al.*, 2000] with peak influence in fall and winter [*Li et al.*,
3 2002]. As European emissions were reduced, the seasonal cycle changed from a peak in October
4 (reflecting dominant influence from fresh European emissions) to a peak in February due to STE.
5 European emission outflow dominates at Barrow (Fig. 11, top row, left panel) from winter to
6 early spring, but Asian emissions become important in late spring [*Liang et al.*, 2004]. The
7 seasonal cycle of CFC-11 gradually decreases in amplitude and shifts from a peak in December
8 during 1985-1989 to a peak in March during 1995-2000, indicating a transition from European-
9 emission-dominated to Asian-emission-dominated. During 2000-2004, the observed seasonal
10 cycle of CFC-11 at Barrow is close to that due to STE, with a maximum in February and a
11 minimum in September. The three sites in the Pacific sector, Trinidad Head, Cape Matatula, and
12 Mauna Loa are, in general, influenced by North American emissions in fall and trans-Pacific
13 transport of Eurasian emissions in spring [*Heald et al.*, 2003; *Liang et al.*, 2004], and hence show
14 a peak in October and a secondary peak in May during the peak emission time. During 2000-
15 2004, amplitudes of observed seasonal cycle of CFC-11 at these sites are greatly reduced with
16 phases approaching those due to STE. The simulated seasonal cycles show an overestimate in
17 spring at these sites as well as Barrow, indicating that the Asian emission used in the simulation
18 is possibly too high.

19 Interestingly, the seasonality of CFC-113 at most of the available sites display a very
20 different signature compared to CFC-11 and CFC-12 during its peak emission time period, 1980-
21 1989. The seasonal maximum occurs during May-July at Mace Head, Trinidad Head, and Cape
22 Grim (Figure 12). This implies that either the usage of CFC-113 during the 1983-89 period has a
23 distinctive seasonal dependence or its regional distribution is very different from that of CFC-11

1 and -12. However, the fact that continuous CFC-113 observations are only available at a few
2 sites before emissions are significantly decreased makes it difficult to address the uniqueness of
3 the seasonality of CFC-113. After 1990, the seasonal cycle of CFC-113 is similar to that of
4 CFC-11 and CFC-12, and gradually reduces to a seasonal cycle that is dominated by STE. The
5 magnitude of the simulated CFC-113 seasonal cycle is smaller than the observed at most sites
6 with additional phase shifts at a few sites, i.e. Barrow, Tutuila, and South Pole, for 2000-2004,
7 implying a missing component from tropospheric transport, as we have discussed in section 4.1.

8

9 **5. Discussion and Summary**

10

11 An emissions-based approach to the ODS forcing of a CCM is a more fundamentally sound
12 technique than constraining a CCM with a mixing ratio boundary condition. The relaxation of
13 the mixing ratio constraint generally assumed in a CCM provides an important step in the
14 evaluation of the governing dynamical and chemical processes that determine the time evolution
15 of ODS. During this evaluation process, ground observations can be used as an important piece
16 of information to validate and improve emission, tropospheric transport, and STE. In the long-
17 run, emissions-based CCM is necessary to accurately predict future ozone recovery. As the first
18 step towards switching from mixing-ratio-based forcing to emissions-based forcing, we have
19 conducted a 45-year emissions-based simulation of the three primary CFCs (CFC-11, -12, and -
20 113) between January 1960 and December 2004 using the GEOS-4 CCM. The simulated mixing
21 ratios and the associated seasonal variations are compared with surface observations at five
22 AGAGE and ten NOAA-GMD sites to evaluate emission sources, photolytic losses, and
23 atmospheric transport processes.

1 The GEOS CCM simulation reproduces well the observed CFC-12 mixing ratios at the
2 surface with average biases of -0.1% in the NH and -0.6% in the SH, indicating a good estimate
3 of emission and atmospheric loss. The simulated CFC-11 in general shows a high bias (5% in
4 the NH and 4% in the SH) and this overestimate increases with time, possibly due to
5 overestimate of emission from banks. If we assume no significant biases with the reported
6 production quantities, the overestimate of CFC-11 emission from banks implies that the current
7 estimate of release rates from plastic foams is too high and significant emissions will extend
8 further into future years than originally expected. The simulated CFC-113 shows a consistent
9 high bias of 18% compared with the observations for the 1983-2004 period. Using a simple
10 budget calculation of atmospheric burden of CFC-113, we deduce that the positive bias of
11 simulated CFC-113 is due to overestimate in emissions. An atmospheric CFC-113 burden
12 calculated with 15% decrease in emission matches well with the observations.

13 The GEOS CCM simulates well the observed inter-hemispheric gradient of CFC-12, but
14 overestimates that of CFC-11 and CFC-113 by 40-50%. Part of the simulation bias is due to a
15 simplification of using the year 2000 spatial emission distribution for the entire simulation period
16 with an additional contribution from the overestimate in emissions.

17 Surface observations of CFCs at many AGAGE and NOAA-GMD sites show significant
18 seasonal variations. Seasonal cycles of CFCs in the lower troposphere are dominated by
19 tropospheric transport of recent emissions during the 1985-1994 period with peak-to-trough
20 amplitude of as much as 6 pptv for CFC-11, 10 pptv for CFC-12, and 3 pptv for CFC-113. Since
21 emissions decrease rapidly after the early 1990s', the amplitude of seasonal variations decreases
22 as the contribution of fresh emissions decreases. The 1995-1999 period marks a transition during
23 which variations due to fresh emissions and STE are equally important with comparable

1 magnitude but distinctive phases. Seasonal cycles of CFCs in the 2000-2004 period are
2 dominated by STE, but tropospheric transport still contributes significantly at many observation
3 sites and affects the amplitude and phase of CFC seasonality. These results are consistent with
4 the conclusions from earlier studies by *Prather et al.* [1987], *Prinn et al.* [2000], and *Nevison et*
5 *al.* [2004]. Seasonal cycles of CFCs due to STE show a late winter/early spring maximum
6 (February-March in NH and September-October in SH) and a summer/fall minimum (July-
7 September in NH and March-May in SH), with amplitudes of ~4-5% (2.0 pptv for CFC-12, 1.6
8 pptv for CFC-11, and 0.4 pptv for CFC-113 during 2000-2004) of absolute mixing ratios are the
9 surface. Individual observation sites show distinctive seasonal cycles of CFCs as governed by
10 seasonal variations of surface emissions transported from various adjacent regions. The GEOS
11 CCM simulates well the seasonal variations of CFCs associated with the STE and the NH-to-SH
12 transport, but less well of that associated with hemispheric transport at a few NH sites, i.e. Mace
13 Head, Trinidad Head, Mauna Loa, and Cape Matatula. The fact that seasonal cycles of CFCs at
14 these sites change significantly as emissions over Europe and North America decrease in the
15 1990s suggests that the seasonality of tropospheric transport of CFCs is dominated by relative
16 emission intensity in the adjacent regions and our simulation bias is possibly due to errors in
17 regional emission distribution.

18 This CFC simulation shows that emissions-based forcing for a CCM can adequately
19 reproduce CFC concentrations. The simulation also shows that the model simulates well the
20 observed magnitude and phase of the seasonal cycles of surface CFCs, providing a simple and
21 useful diagnostic to evaluate atmospheric mean circulation in CCMs. In addition, seasonality of
22 long-lived atmospheric trace gases like CFCs in the lower troposphere varies accordingly as
23 emissions change. Even when emissions become small, the seasonality due to tropospheric

1 transport of recent emissions still contributes significantly to altering the magnitude and phase of
2 seasonal cycles. Therefore, the observed seasonal cycle of long-lived atmospheric trace gases
3 provides an additional independent piece of information, in addition to atmospheric
4 concentrations, to constrain a top-down emission inventory. Regional tagging technique and
5 inverse modeling have been used extensively in the past decade to improve the emission
6 inventory of anthropogenic pollutants such as CO [e.g. *Bey et al.*, 2001; *Palmer et al.*, 2003].
7 Applying such techniques in CCMs or Chemical Transport Models with emissions-based forcing
8 and using observed seasonality as constraints provides a useful tool in not only obtaining a top-
9 down estimate of global emissions of CFCs but also a reasonable regional emission distribution.
10 This method will be particularly useful for long-lived atmospheric trace gases with less-well
11 understood sources and/or sinks, i.e. N₂O, CH₄, CO₂.

12

13

14 *Acknowledgements.* This research was supported by an appointment to the NASA Postdoctoral
15 Program at the Goddard Space Flight Center, administered by Oak Ridge Associated
16 Universities through a contract with NASA.

1 **References.**

- 2
3
4 AFEAS (Alternative Fluorocarbons Environmental Acceptability Study) (1995), *Production,*
5 *Sales and Atmospheric Releases of Fluorocarbons through 1993*, Arlington, VA, USA.
6 AFEAS (Alternative Fluorocarbons Environmental Acceptability Study) (2001), *Production,*
7 *Sales and Atmospheric Releases of Fluorocarbons through 2000*, Arlington, VA, USA.
8 Austin, J., and F. Li (2006), On the relationship between the strength of the Brewer-Dobson
9 circulation and the age of stratospheric air, *Geophys. Res. Lett.*, *33*,
10 doi:10.1029/2006GL026867.
11 Bey, I., D. J. Jacob, J. A. Logan, and R. M. Yantosca (2001), Asian chemical outflow to the
12 Pacific: Origins, pathways and budgets, *J. Geophys. Res.*, *106*, 23,097-23,114.
13 Bloom, S., et al. (2005), The Goddard Earth Observation System Data Assimilation System,
14 GEOS DAS version 4.0.3: Documentation and validation, *NASA Tech. Memo.*, *TM-2005-*
15 *104606*, vol. 26, pp 166.
16 Bowman, K. P., and P. J. Cohen (1997), Interhemispheric Exchange by Seasonal Modulation of
17 the Hadley Circulation, *J. Atmos. Sci.*, *54*, 2045-2059.
18 Butchart, N., et al. (2006), Simulations of the anthropogenic change in the strength of the
19 Brewer-Dobson circulation, *Clim. Dyn.*, *27*, 727-741.
20 Butchart, N., and A. A. Scaife (2001), Removal of chlorofluorocarbons by increased mass
21 exchange between the stratosphere and troposphere in a changing climate, *Nature*, *410*,
22 799-802.
23 Cape, J. N., J. Methven, and L. E. Hudson (2000), The use of trajectory cluster analysis to
24 interpret trace gas measurements at Mace Head, Ireland, *Atmos. Environ.*, *34*, 3651-3663.
25 Daniel, J. S., G. J. M. Velders, S. Solomon, M. McFarland, and S. A. Montzka (2007), Present
26 and future sources and emissions of halocarbons: Toward new constraints, *J. Geophys. Res.*,
27 *112*, D02301, doi:10.1029/2006JD007275.
28 Douglass, A. R., C. J. Weaver, R. B. Rood, and L. Coy (1996), A three-dimensional simulation
29 of the ozone annual cycle using winds from a data assimilation system, *J. Geophys. Res.*, *101*
30 (D1), 1463-1474.
31 Douglass, A. R., R. S. Stolarski, M. R. Schoberl, C. H. Jackman, M. Gupta, P. A. Newman, J. E.
32 Nielsen, and E. L. Fleming (2007), The relationship of loss, mean age and the distribution of
33 CFCs to model circulation and implications for atmospheric lifetimes, manuscript in
34 preparation.
35 Environmental Protection Agency (EPA), *Economic implications of regulating*
36 *chlorofluorocarbon emissions from nonaerosol applications*, *EPA Rep. EOA-560/12-80-001*,
37 U.S. Environ. Prot. Agency, Washington, D.C., 1980.
38 Eyring, V., et al. (2006), Assessment of temperature, trace species, and ozone in chemistry-
39 climate model simulations of the recent past, *J. Geophys. Res.*, *111*, D22308,
40 doi:10.1029/2006JD007327.
41 Fisher, D., and P. Midgley (1996), The production and release to the atmosphere of CFCs 113,
42 114 and 115, *Atmos. Environment.*, *27A*, 271-276.
43 Gupta, M. L., R. P. Turco, C. R. Mechoso, and J. A. Spahr (2001), Online simulations of passive
44 chemical tracers in the university of California, Los Angeles, atmospheric general circulation
45 model: 1. CFC-11 and CFC-12, *J. Geophys. Res.*, *106*(D12), 12,401-12,418,
46 doi:10.1029/2000JD900819.

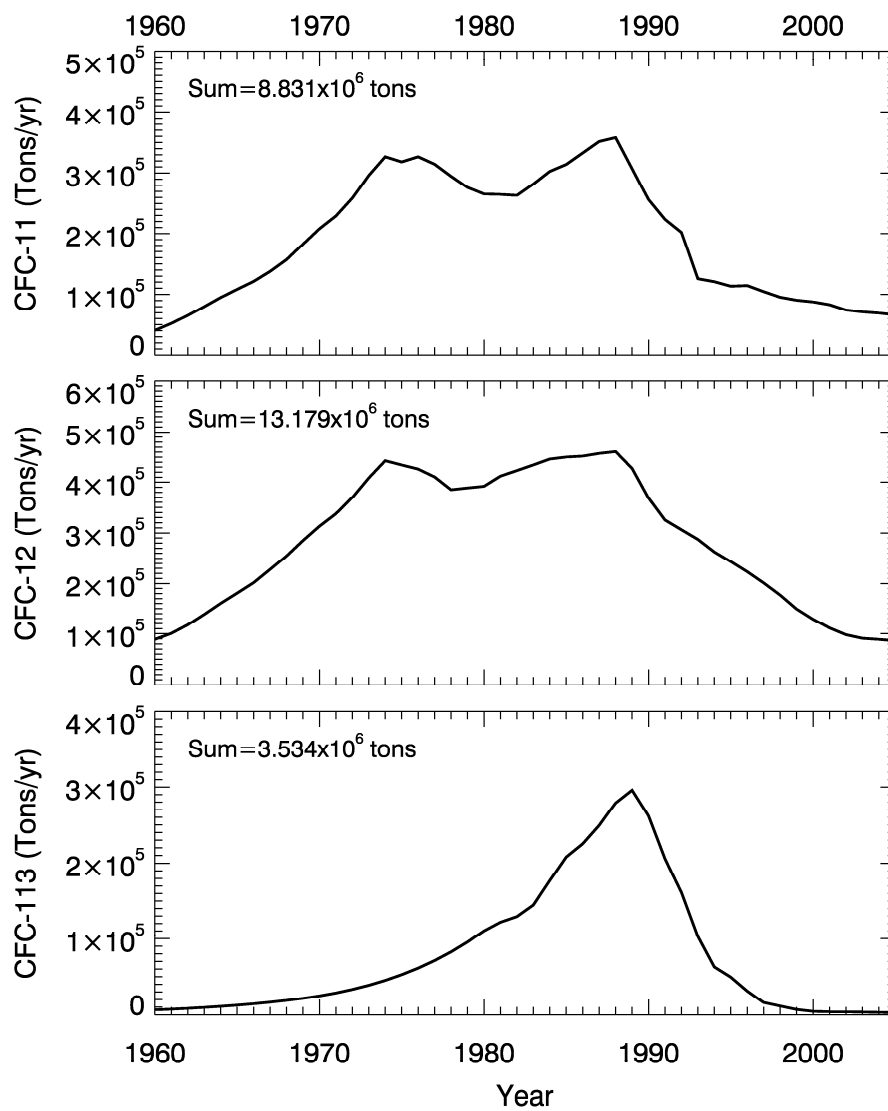
- 1 Heald, C. L., et al. (2003), Asian outflow and transpacific transport of carbon monoxide and
2 ozone pollution: An integrated satellite, aircraft and model perspective, *J. Geophys. Res.*,
3 *108*(D24), 4804, doi:10.1029/2003JD003507.
- 4 Holton, J. R., P. H. Haynes, M. E. McIntyre, A. R. Douglass, R. B. Rood, and L. Pfister (1995),
5 Stratosphere-Troposphere Exchange, *Rev. Geophys.*, *33*(4), 403-439.
- 6 Intergovernmental Panel on Climate Change/Technology and Economic Assessment Panel
7 (2005), *IPCC Special Report: Safeguarding the Ozone Layer and the Global Climate System:
8 Issues Related to Hydrofluorocarbons and Perfluorocarbons*, 478 pp., Cambridge Univ.
9 Press, New York.
- 10 Jiang, X., W. L. Ku, R.-L. Shia, Q. Li, J. W. Elkins, R. G. Prinn, and Y. L. Yung (2007),
11 Seasonal cycle of N₂O: Analysis of data, *Global Biogeochem. Cycles*, *21*, GB1006,
12 doi:10.1029/2006GB002691.
- 13 Law, K. S., and A. Stohl. (2007), Arctic Air Pollution: Origins and Impacts, *Science*, *315*, 1537-
14 1540, doi:10.1126/science.1137695.
- 15 Li Q., D. J. Jacob, I. Bey, P. I. Palmer, B. N. Duncan, B. D. Field, R. V. Martin, A. M. Fiore, R.
16 M. Yantosca, D. D. Parrish, P. G. Simmonds, and S. J. Oltmans (2002), Transatlantic
17 transport of pollution and its effects on surface ozone in Europe and North America, *J.
18 Geophys. Res.*, *107*(D13), doi:10.1029/2001JD001422.
- 19 Liang, Q., L. Jaeglé, D. A. Jaffe, P. Weiss-Penzias, A. Heckman, and J. A. Snow (2004), Long-
20 range transport of Asian pollution to the northeast Pacific: Seasonal variations and transport
21 pathways of carbon monoxide, *J. Geophys. Res.*, *109*, D23S07, doi:10.1019/2003JD004402.
- 22 McCulloch, A., P. Ashford, and P. M. Midgley (2001), Historic Emissions of
23 Fluorotrichloromethane (CFC-11) Based on a Market Survey, *Atmos. Environ.*, *35*(26), 4387-
24 4397.
- 25 McCulloch, A., P. M. Midgley, and P. Ashford (2003), Releases of Refrigerant Gases (CFC-12,
26 HCFC-22, and HFC-134a) to the Atmosphere, *Atmos. Environ.*, *37*(7), 889-902.
- 27 Montzka, S. A., J. H. Butler, J. W. Elkins, T.M. Thompson, A. D. Clarke, and L. T. Lock (1999),
28 Present and future trends in the atmospheric burden of ozone-depleting halogens, *Nature*,
29 *398*(6729), 690-694.
- 30 Nevison, C. D., D. E. Kinnison, and R. F. Weiss (2004), Stratospheric influences on the
31 tropospheric seasonal cycles of nitrous oxide and chlorofluorocarbons, *Geophys. Res. Lett.*,
32 *31*, L20103, doi:10.1029/2004GL020398.
- 33 Olsen, M. A., M. R. Schoeberl, and A. R. Douglass (2004), Stratosphere-troposphere exchange
34 of mass and ozone, *J. Geophys. Res.*, *109*, D24114, doi:10.1029/2004JD005186.
- 35 Palmer, P. I., et al. (2003), Inverting for emissions of carbon monoxide from Asia using aircraft
36 observations over the western Pacific, *J. Geophys. Res.*, *108*(D21), 8828,
37 doi:10.1029/2003JD003397.
- 38 Pawson, S., R. S. Stolarski, A. R. Douglass, P. A. Newman, J. E. Nielsen, S. M. Frith, and M. L.
39 Gupta (2007), Goddard Earth Observing System Chemistry-Climate Model Simulations of
40 Stratospheric Ozone-Temperature Coupling Between 1950 and 2005, submitted to *J.
41 Geophys. Res.-Atmospheres*.
- 42 Prather, M., M. McElroy, S. Wofsy, G. Russell, and D. Rind (1987), Chemistry of the global
43 troposphere: Fluorocarbons as tracers of air motion, *J. Geophys. Res.*, *92*, 6579-6613.
- 44 Prinn, R. G., et al. (2000), A history of chemically and radiatively important gases in air deduced
45 from ALE/GAGE/AGAGE, *J. Geophys. Res.*, *105*, 17,751-17,792.

- 1 Shia, R.-L., M.-C. Liang, C. E. Miller, and Y. L. Yung (2006), CO₂ in the upper troposphere:
2 Influence of stratosphere-troposphere exchange, *Geophys. Res. Lett.*, *33*, L14814,
3 doi:10.1029/2006GL026141.
- 4 Simmonds, P. G., S. Seuring, G. Nickless, and R. G. Derwent (1997), Segregation and
5 Interpretation of Ozone and Carbon Monoxide Measurements by Air Mass Origin at the TOR
6 Station Mace Head, Ireland from 1987 to 1995, *J. Atmos. Chem.*, *28*, 45-59.
- 7 Stohl, A. (2006), Characteristics of atmospheric transport into the Arctic troposphere, *J. Geophys.*
8 *Res.*, *111*, D11306, doi:10.1029/2005JD006888, 2006.
- 9 Stohl, A., S. Eckhardt, C. Forster, P. James, and N. Spichtinger (2002), On the pathways and
10 timescales of intercontinental air pollution transport, *J. Geophys. Res.*, *107*(D23), 4684,
11 doi:10.1029/2001JD001396.
- 12 Stolarski, R. S., A. R. Douglass, S. Steenrod, and S. Pawson (2006b), Trends in stratospheric
13 ozone: Lessons learned from a 3D chemical transport model, *J. Atmos. Sci.*, *63*, 1028-1041.
- 14 Thompson, T. M., et al. (2004), Halocarbons and other atmospheric trace species, Summary Rep.
15 27 2002-2003, edited by R. C. Schnell et al., pp. 115-135, Clim. Monit. Diagn. Lab., U.S.
16 Dep. Of Commer., Boulder, Colo.
- 17 Waugh, D. W., S. E. Strahan, and P. A. Newman (2007), Sensitivity of stratospheric inorganic
18 chlorine to differences in transport, *Atmos. Chem. Phys.*, *7*, 4935-4941.
- 19 World Meteorological Organization (WMO) (2003), *Scientific assessment of ozone depletion:*
20 *2002, Rep. 47*, Global Ozone Research and Monitoring Project, Geneva.
- 21 World Meteorological Organization (WMO) (2007), *Scientific assessment of ozone depletion:*
22 *2006, Rep. 50*, Global Ozone Research and Monitoring Project, Geneva.

1 **Table 1.** Geographical and measurement information of the AGAGE and NOAA-GMD
 2 observation sites.
 3

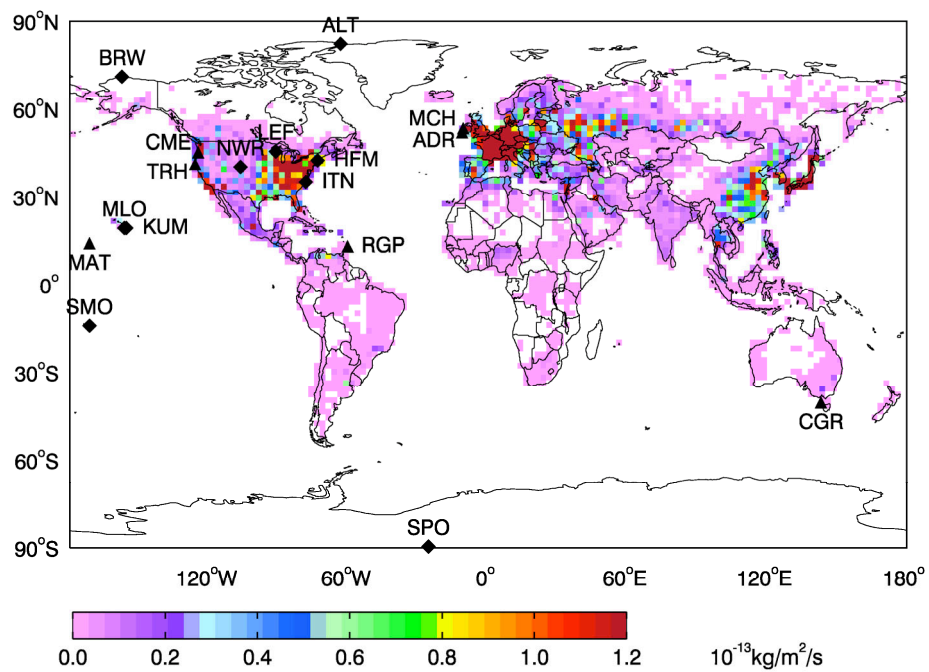
	Station	Longitude	Latitude	Altitude	Measurements	Time Period	
NH	AGAGE	Adrigole	10.0°W	53.0°N	50m		1979-1983
		Mace Head	9.5°W	53.4°N	25m		1987-2004
		Cape Meares	123.6°W	45.3°N	30m	Continuous	1979-1989
		Trinidad Head	124.9°W	41.3°N	120m	Gas Chromatograph (GC)	1995-2004
		Ragged Point	59.3°W	13.1°N	45m		1978-2004
		Cape Matatula	170.3°W	14.2°N	42m		1978-2004
	NOAA-GMD	Alert	62.3°W	82.3°N	210m	Weekly Flask	1988-2004
		Barrow	156.4°W	71.2°N	8m	Weekly Flask, CATS, RITS	1977-2004
		Park Falls	90.2°W	45.6°N	868m	Weekly Flask	1996-2004
		Harvard Forest	72.2°W	42.5°N	340m	Weekly Flask	1995-2004
		Niwot Ridge	105.4°W	40.3°N	3475m	Flask, CATS, RITS	1977-2004
		Grifton	77.2°W	35.2°N	9m	Weekly Flask	1995-1999
		Cape Kumukahi	154.5°W	19.3°N	3m	Weekly Flask	1995-2004
Mauna Loa	155.4°W	19.3°N	3397m	Weekly Flask, CATS, RITS	1977-2004		
SH	AGAGE	Cape Grim	144.4°E	40.4°S	94m	Continuous GC	1978-2004
	NOAA-GMD	Tutuila	170.3°W	14.2°S	42m	Weekly Flask, CATS, RITS	1977-2004
		South Pole	24.5°W	89.6°S	2810m	Weekly Flask, CATS, RITS	1977-2004

- 1 **Figure 1.** Annual global emissions of CFC-11 (top), CFC-12 (middle), and CFC-113 (bottom)
2 between 1960 and 2004. The total 45-year emission sums are on the top of each panel.
3



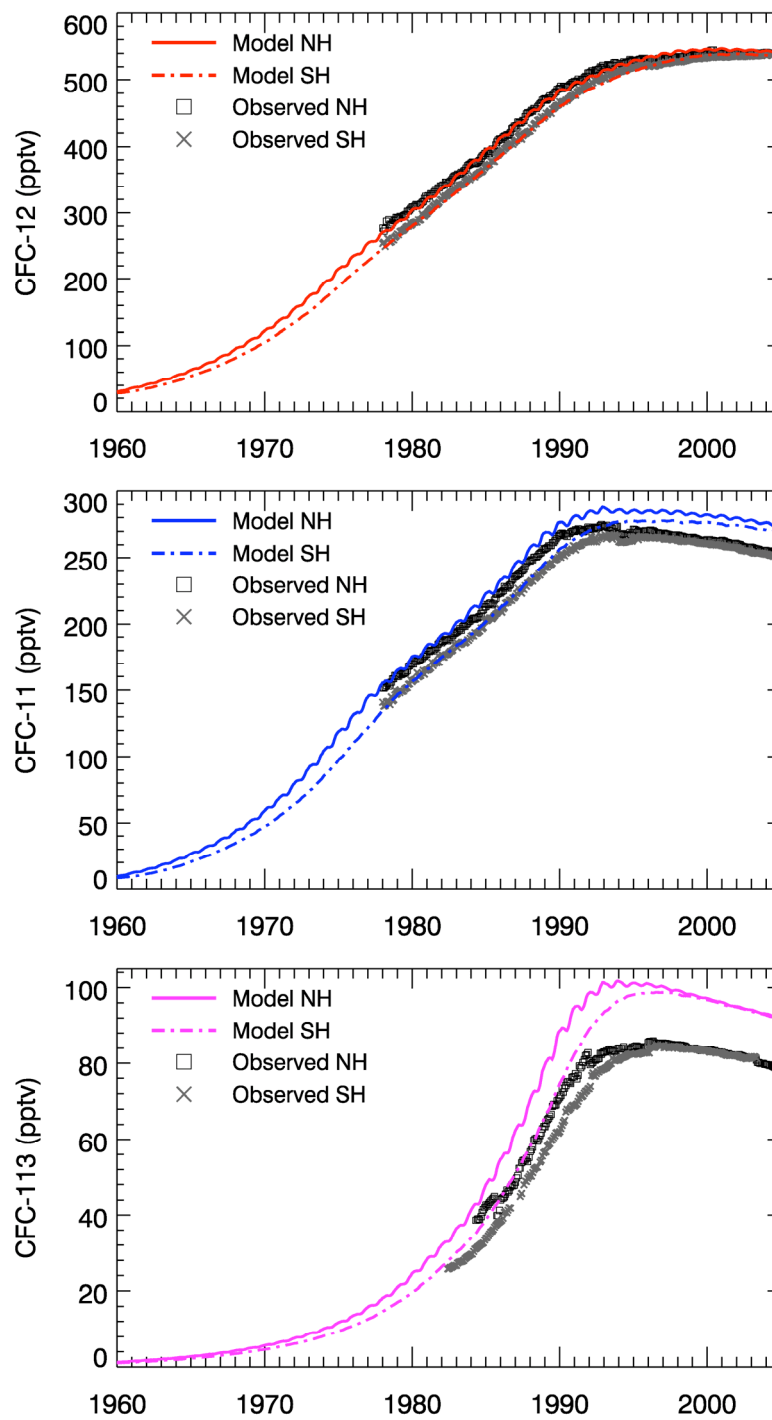
1 **Figure 2.** Global emissions of CFC-11 for 2000. The black symbols (triangles for AGAGE
2 stations and diamonds for NOAA-GMD stations) mark the location of the ground observation
3 sites.

4



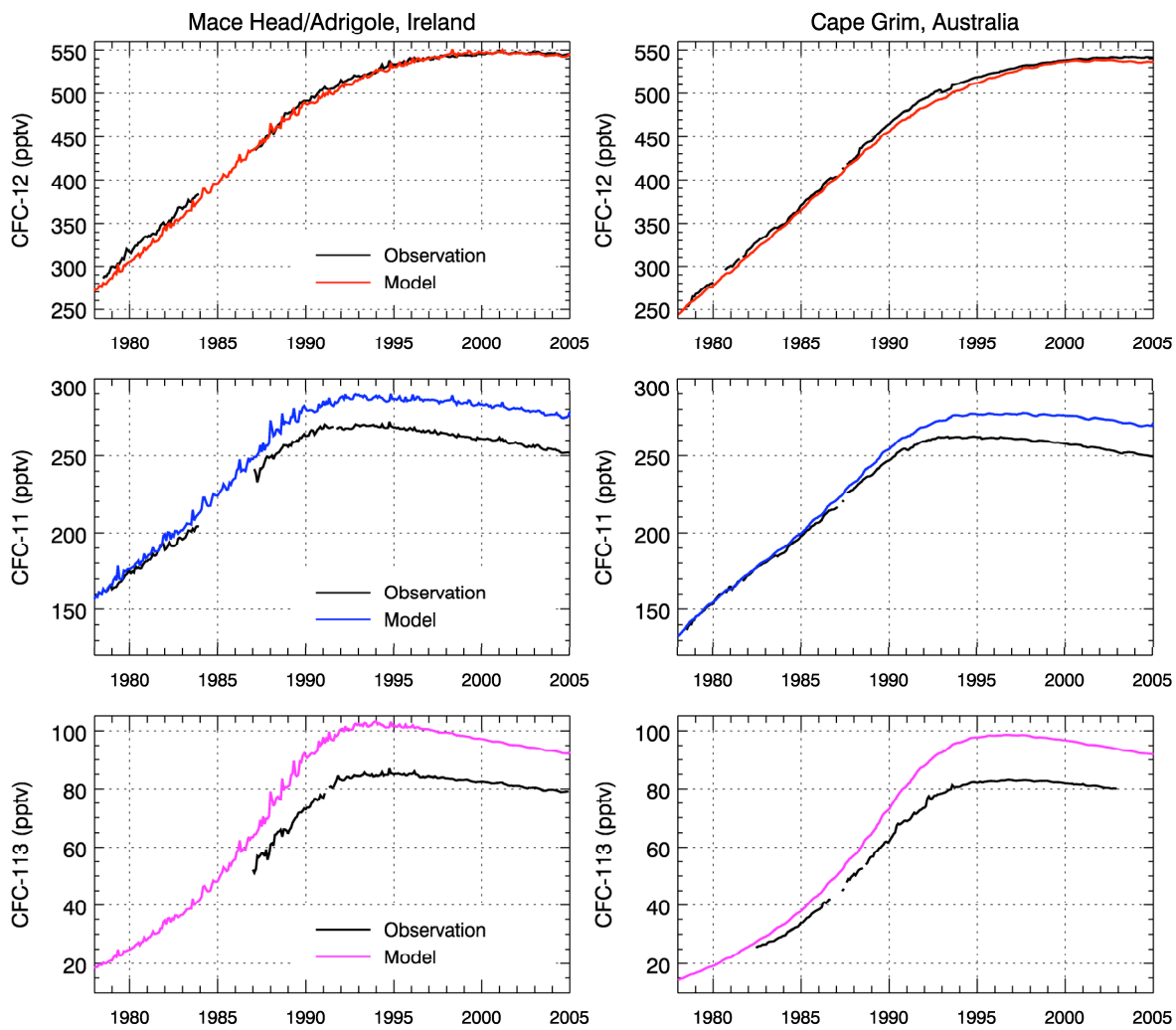
5

1
2 **Figure 3.** The observed (black squares for NH, gray crosses for SH) and modeled (solid lines for
3 NH, dashed lines for SH) hemispheric averaged monthly mean surface CFC-12 (red), CFC-11
4 (blue), and CFC-113 (magenta) mixing ratios between January 1960 and December 2004.
5



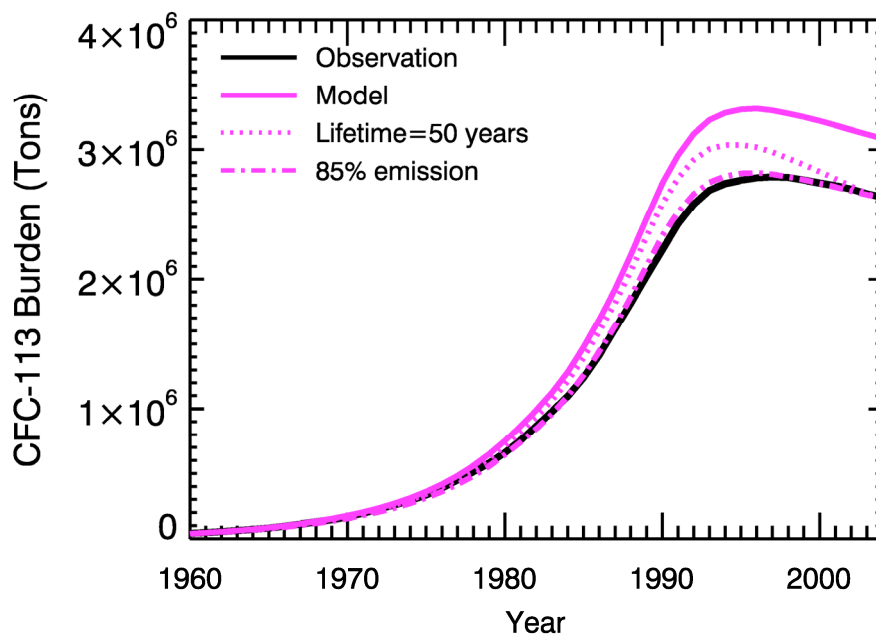
6
7

1 **Figure 4.** Timeseries of observed (black) and modeled CFC-12 (red), CFC-11 (blue) and CFC-
2 113 (magenta) at Mace Head/Adrigole, Ireland, and Cape Grim, Australia.



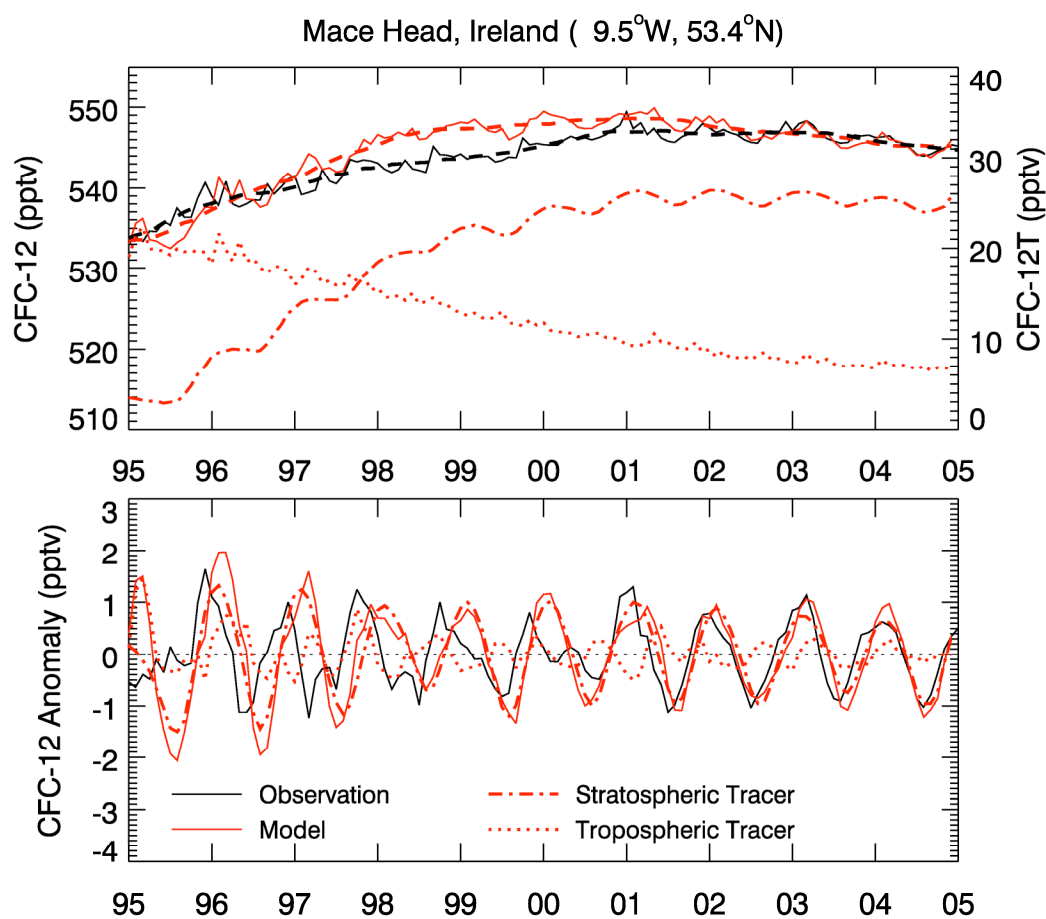
3
4
5

1 **Figure 5.** Global atmospheric burden of CFC-113 between 1960 and 2004. The simulated and
2 observation-inferred burdens are plotted as solid black and magenta lines, respectively. Two
3 additional projected global burdens are also shown: one calculated with a CFC-113 lifetime of 50
4 years (dotted line) and the other with 85% of the emission (dash-dotted line).



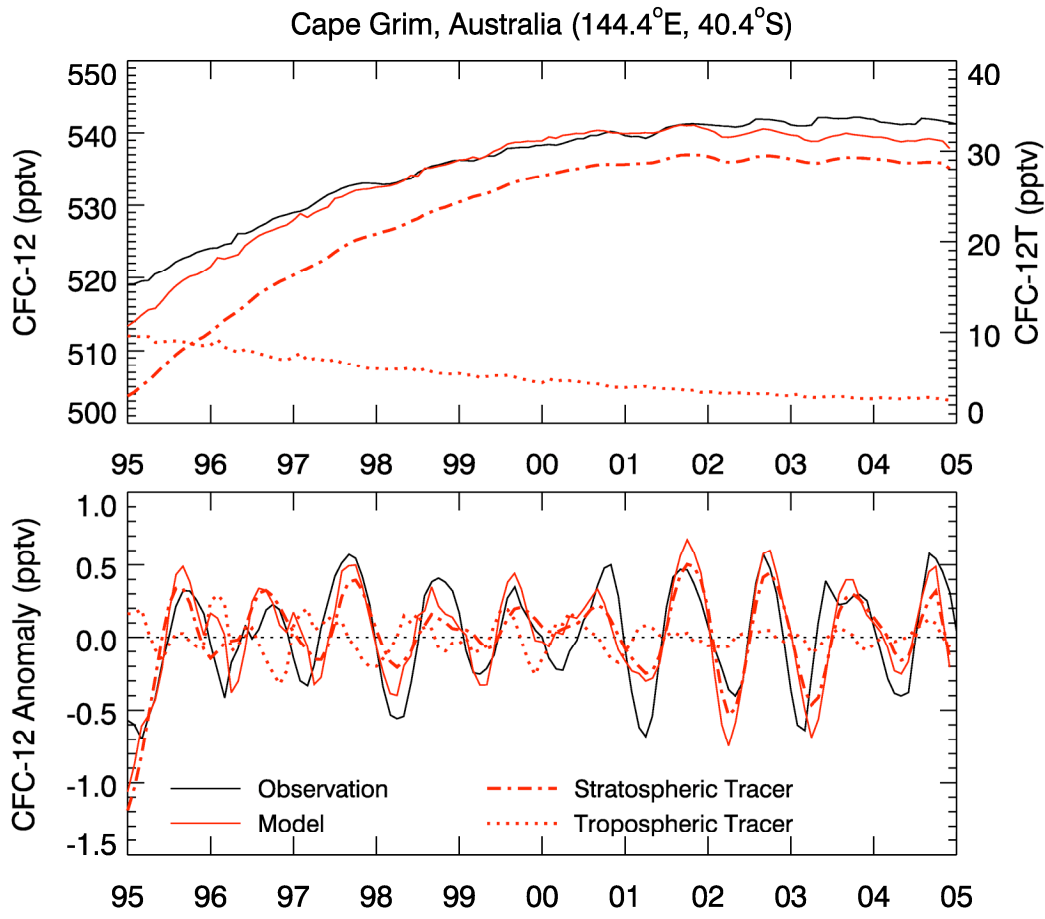
5

1 **Figure 6a.** Top: Monthly mean time series of observed (black thin line) and simulated (red thin line)
 2 CFC-12 at Mace Head, Ireland, between January 1995 and December 2004. The thick
 3 dashed lines (black for observation and red for model) are the long-term trend determined using
 4 a 13-month boxcar average algorithm. The model stratospheric CFC (CFC-12S, red dash-dotted
 5 line) and tropospheric CFC (CFC-12T, red dotted line) are also shown. Note that CFC-12T
 6 follows a different scale on the right of the panel. The de-trended monthly anomalies of observed
 7 CFC-12, simulated CFC-12, CFC-12S and CFC-12T are shown in the bottom panel.
 8



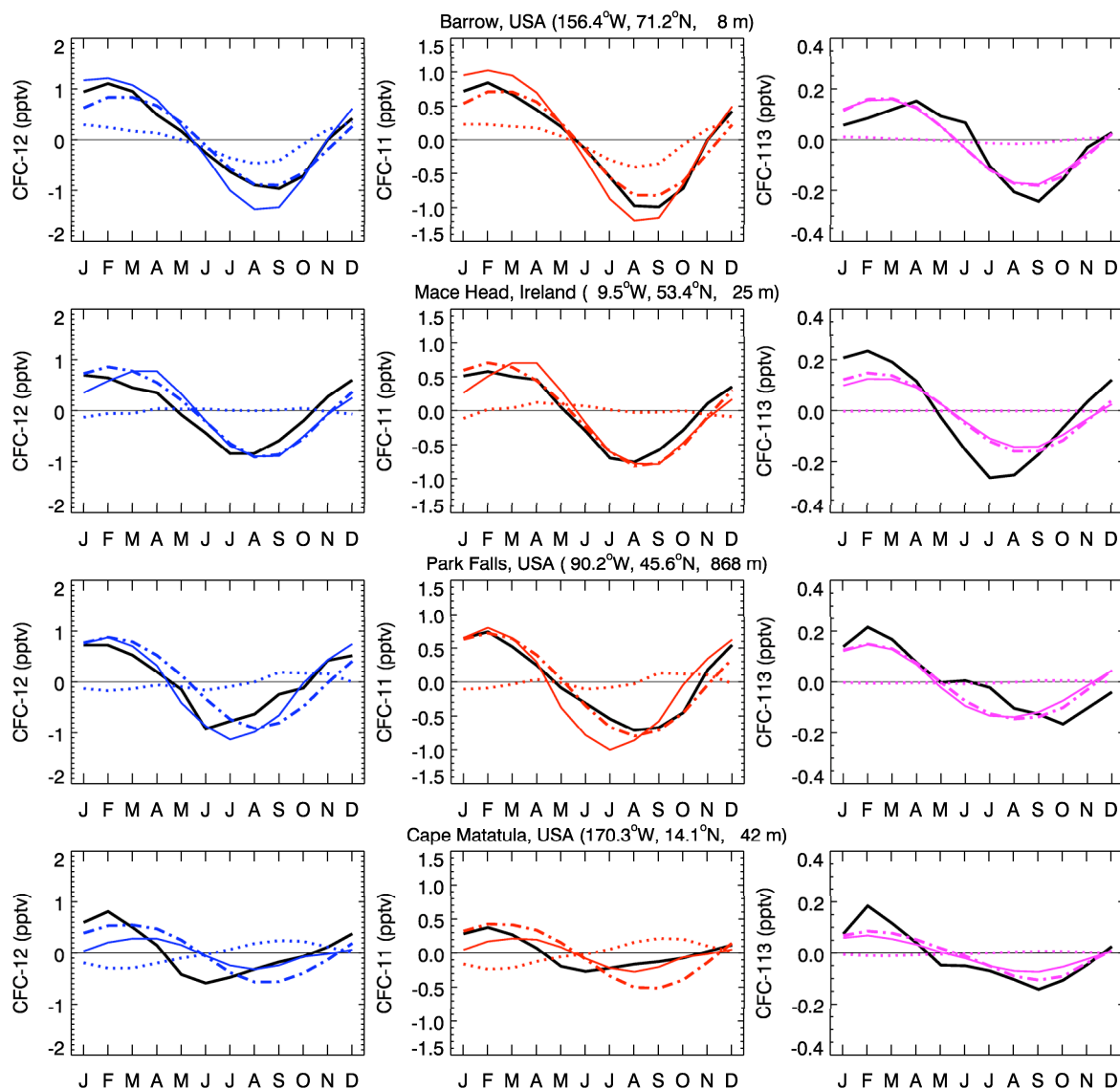
9
 10
 11

1 **Figure 6b.** Same as Figure 6a but for Cape Grim and the long-term trends are not shown for
2 better visibility of the seasonal cycles.

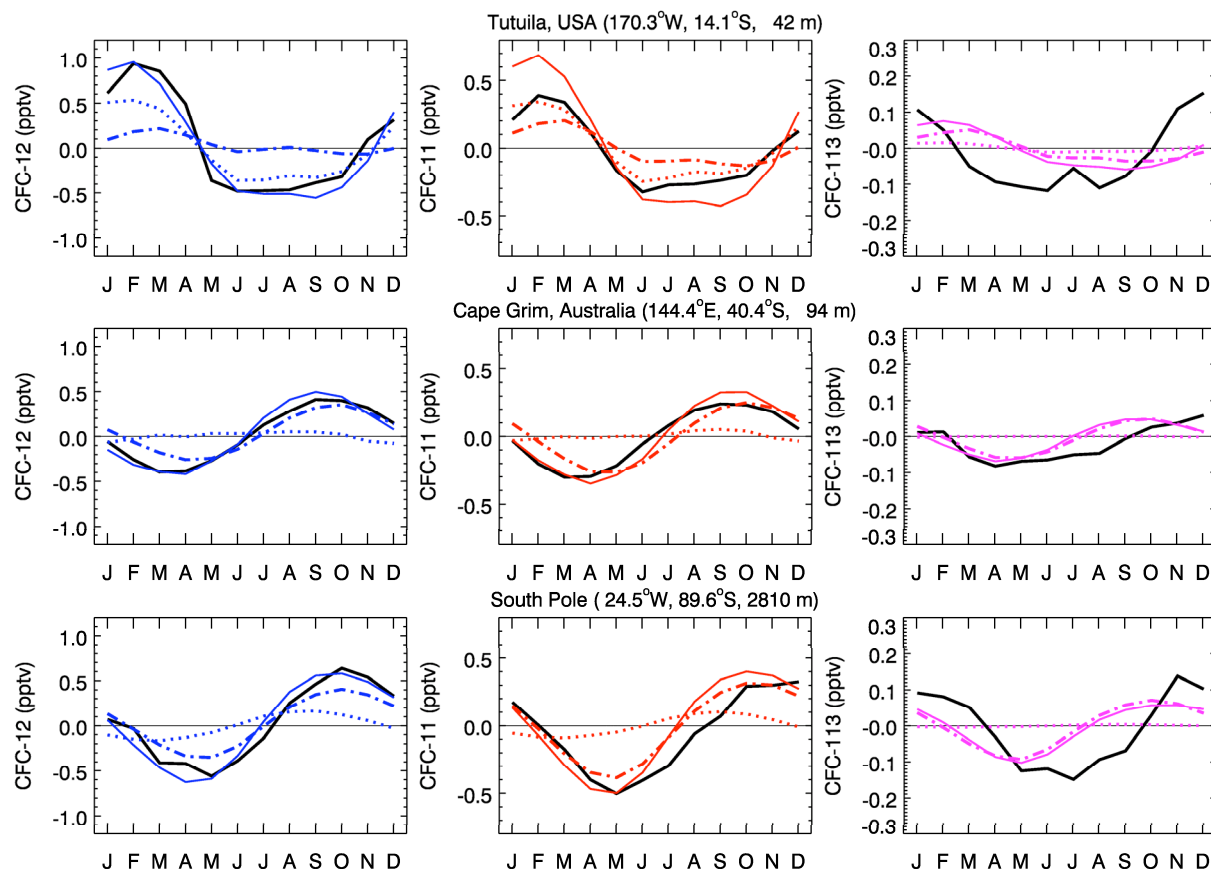


3

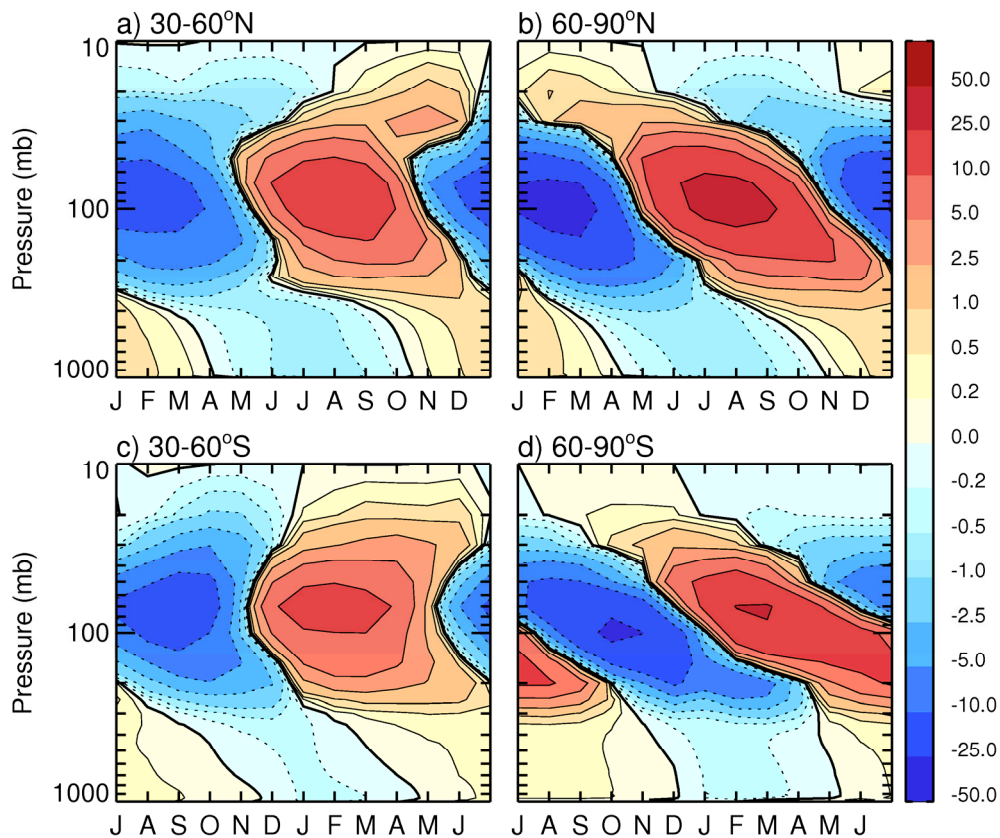
1 **Figure 7a.** The 5-year averaged seasonal cycles of observed (black solid lines) and simulated
 2 CFCs (color solid lines), and the two tagged CFC tracers (color dash-dotted lines for the
 3 stratospheric tracers and color dotted lines for the tropospheric tracers) for 2000-2004 at four
 4 northern hemispheric stations: Barrow, Mace Head, Park Falls, and Cape Matatula.
 5



1 **Figure 7b.** Same as Figure 8a but for three southern hemispheric stations: Tutuila, Cape Grim, and South Pole.
 2

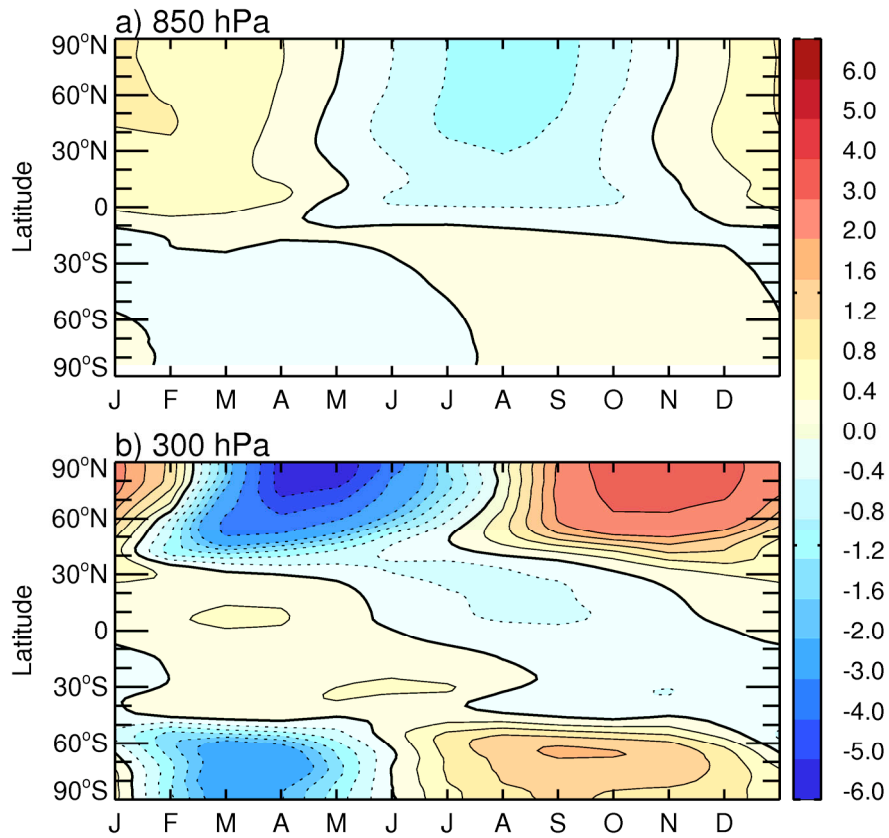


1 **Figure 8.** Time-pressure cross section of monthly mean anomalies of zonal mean CFC-12S
2 averaged between (a) 30-60°N, (b) 60-90°N, (c) 30-60°S, and (d) 60-90°S. The monthly mean
3 anomalies are obtained by apply a 13-month high-pass filter and averaged between 1995 and
4 2004.
5



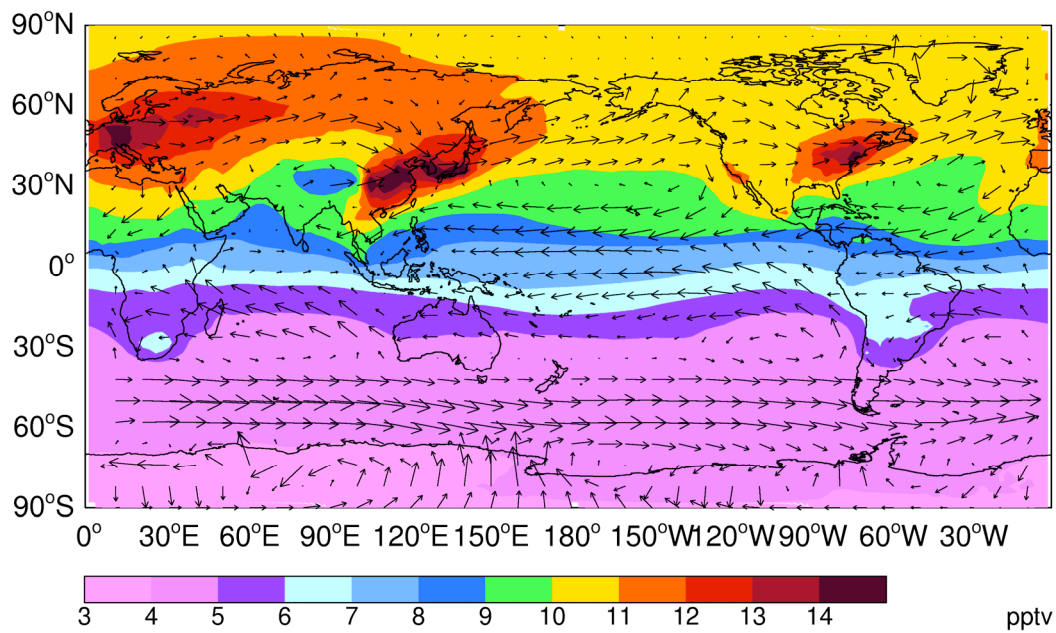
6
7

- 1 **Figure 9.** Monthly evolution of zonal mean CFC-12S anomalies between 90°S-90°N at (a)
- 2 850hPa and (b) 300hPa. The monthly mean anomalies are obtained by apply a 13-month high-
- 3 pass filter and averaged between 1995 and 2004.



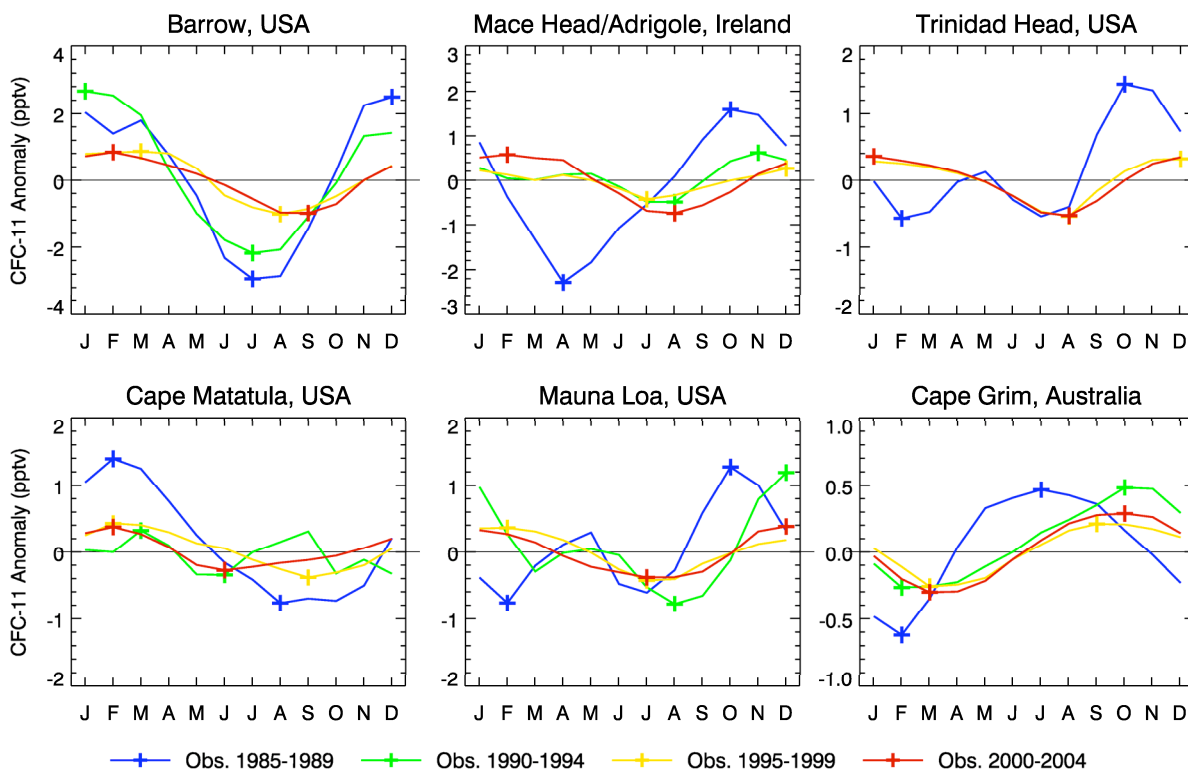
4
5

- 1 **Figure 10.** Global distribution of the simulated tropospheric tracer, CFC-12T (color contours)
- 2 and winds (vectors) averaged between 0-2 km for 2000.



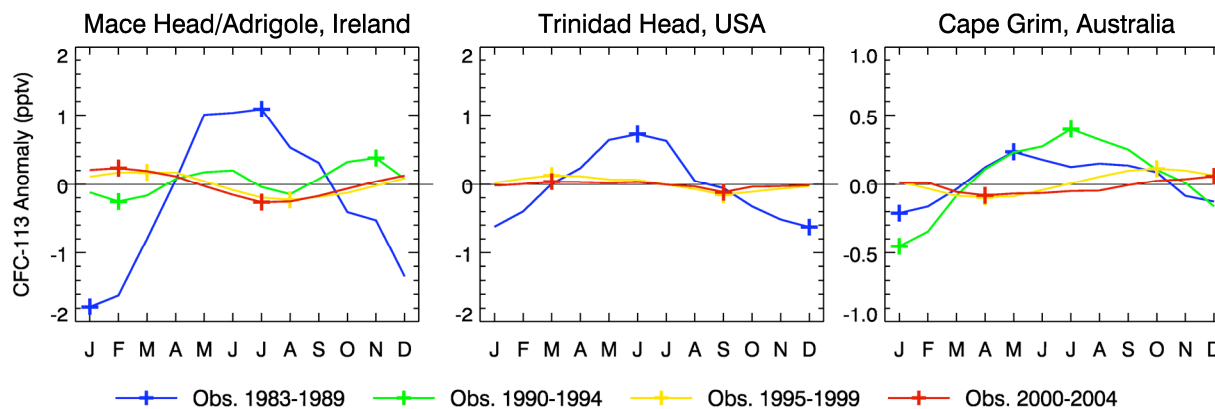
3
4

1 **Figure 11.** 5-year averaged seasonal cycles of observed CFC-11 at 6 AGAGE/GMD sites for
 2 1985-1989 (blue), 1990-1994 (green), 1995-1999 (yellow), and 2000-2004 (red), respectively.
 3 Months with minimum and maximum concentrations are marked with pluses.



4
 5
 6
 7
 8
 9
 10

Figure 12. Same as Figure 11 but for CFC-13 at Mace Head/Adrigole, Trinidad Head, and Cape Grim.



11
 12
 13